

# ON-ORBIT MODULATION TRANSFER FUNCTION ESTIMATION FOR BiLSAT IMAGERS

U. M. Leloglu\*, E. Tunali

TUBITAK-SPACE, ODTU Kampusu, 06531 Ankara Turkey - (leloglu, tunali)@bilten.metu.edu.tr

Commission I, WG I/6

**KEY WORDS:** Modeling, Resolution, Optical, Sensors, Small satellites, Cal/Val

## ABSTRACT:

BiLSAT, launched to its sun-synchronous orbit on 27.09.2003, is a 129 Kg small satellite carrying a panchromatic camera and a 4-band multispectral camera with Ground Sampling Distances (GSD) 12.6 m and 28 m, respectively. The multispectral camera is composed of 4 totally independent cameras. All five refractive optic cameras have 2048 by 2048 frame CCDs as sensors. The overall Modulation Transfer Functions (MTF) of the imaging systems are very important for characterization of imagers. In this study, the MTF of BiLSAT imagers are calculated using two different methods.

The first method for image-based MTF determination uses sharp linear edges for estimating the Edge Spread Function (ESF), from which Point Spread Function (PSF) is obtained by differentiation. A man-made high-contrast almost linear structure is used as imaging target. For precise detection of the edges, a 2D edge model is fitted to manually picked linear edge and the root-mean-square (RMS) difference between the image and the model is minimized by gradient search. Then, a parametric curve fitting is performed using a new parametric model. The PSF and MTF are obtained after differentiation and Fourier transformation, respectively.

Second method is based on comparing BiLSAT images to high-resolution IKONOS images whose PSF is already known. The blur function that minimizes the RMS difference between the registered images is estimated. Image registration, blur estimation and radiometric correction parameter estimation are performed simultaneously. The fact that the images are taken with 3 months time difference and from slightly different angles cause difficulties. Small and almost planar areas are chosen to avoid parallax effects. Finally, the results obtained by two different methods are compared and the results are discussed.

## 1. INTRODUCTION

The spatial resolution of spaceborne imaging systems is one of the most important parameters defining the performance of the imager. Although the resolution of imagers is generally expressed in terms of the ground sampling distance, this is meaningful when the system Modulation Transfer Function (MTF) is specified. Most of the time, the MTF of imagers are measured before the launch, however, they may change due to vacuum, vibration during launch or change in material properties in time. For that reason, on-orbit MTF determination is necessary to have actual and up-to-date performance of spaceborne imagers.

BiLSAT earth observing satellite has been built in the framework of a technology transfer program between SSTL, Guildford, UK and TUBITAK-SPACE (Former TUBITAK-BILTEN), Ankara, Turkey. Since its launch on Sept. 27, 2003 to its sun-synchronous orbit at 686 km, it is being operated from the ground station in Ankara. BiLSAT has a panchromatic camera with a 12.6 m ground sampling distance (GSD), and four separate cameras sensitive to red, green, blue and NIR bands, together forming a multi-spectral camera with a 28 m GSD. All 5 cameras have 2048 x 2048 frame CCD sensors (See (Yüksel, 2004) for more info. on the mission and (Friedrich, 2006) for imaging system). Since each camera is

completely independent, the MTF for each needs to be estimated.

In this study, the MTF of BiLSAT imagers are calculated using two different methods. The first method uses sharp linear edges for estimating the Edge Spread Function (ESF) and hence the Point Spread Function (PSF) and MTF. Second method is based on comparing BiLSAT images to IKONOS images whose PSF is already known. After MTF determination by both methods, results are compared. In Section 2, on-orbit MTF determination methods are reviewed. The methods used for BiLSAT and obtained results are presented in Section 3 and the study is concluded in Section 4.

## 2. ON-ORBIT MTF DETERMINATION METHODS

Most of the methods for determining MTF from spaceborne images use specific artificial or natural targets on the ground (If available, on-board targets can also be used (Braga, 2000)). Frequently these targets are point light sources, edges or rectangular pulses. From images of light sources (spot lights or mirrors) the PSF of the imager is directly available, however, it is undersampled so a parametric fit is necessary (Léger, 1994) or the PSF should be reconstructed using many such images with different sub-pixel positions of the impulse (Rauchmiller, 1998). Once the PSF is found, the magnitude of the Fourier

---

\* Corresponding author.

transform (FT) of PSF gives us the MTF. Images of roads, bridges etc. over a uniform background can be modeled as a rectangular pulse along the direction perpendicular to it. When the FT of the response of the imager to the pulse is divided by the FT of the pulse itself, the MTF is obtained. But since the FT of a rectangular pulse is a *sinc* function, it has zeros around which MTF cannot be estimated reliably so the rectangle size should be chosen carefully. If a linear and sharp edge with uniform areas on both sides can be imaged, then the Edge Spread Function (ESF) (Tatian, 1965) can be found along the direction perpendicular to the edge, which is the system response to a step function whose derivative gives the PSF. Only one scan line perpendicular to the edge is not sufficient since the ESF is undersampled. So, many pixels along the edge are projected on a single line perpendicular to the edge to obtain as many as sample points necessary for reconstructing the ESF. When the edge method is used, precise determination of edge angle and position is very important. Because, when there is an error in the edge angle, the projections of points along the edge will shift and the computed PSF will be larger than it actually is. One method for avoiding this problem is to fit cubic polynomials to each row (assuming that the edge is almost vertical) for finding subpixel edge position along that row and subsequently to fit a straight line to these sub-pixel edge positions (Helder, 2002). Another approach presented in (Kohm, 2004) is to minimize the differences between the data points and the fitted ESF by fine-tuning the edge orientation.

Once the samples on the ESF are obtained, parametric or non-parametric approaches can be taken. Parametric approaches assume a known model for the ESF and the parameters of the model that fits the data best, are estimated. Error function (i.e. Gaussian PSF), polynomials (e.g. Forster, 1994) and superposition of 3 sigmoids (Blonski, 2002) are some examples. Note that, in (Blonski, 2002), the ESF parameters are determined simultaneously with edge position and angle, so this phase is combined with the previous one. Parametric models are less sensitive to noise, however, any deviation from assumed model creates errors.

In non-parametric methods, the ESF is differentiated numerically. However, since the samples of the ESF are not equally spaced, some form of interpolation is necessary. Cubic spline interpolation (Choi, 2003b), LOESS (Kohm, 2004) and Savitzky-Golay Helder-Choi filtering (Helder, 2003) are examples to successful methods.

It is also possible to find MTF from images without using specific targets. For example, in (Luxen, 2002), a method for blind determination of PSF from any image containing many sharp edges under the assumption of Gaussian PSF is described. Using artificial neural networks (Delvit, 2004) is another approach. However, most frequently used method is comparing the images of the same area from the imager under consideration and an imager with a known MTF. It is best if the imagers are on-board of the same satellite and they are taken simultaneously.

To be able to compare the images, they need to be registered accurately first. If the imagers are on the same satellite, the transformation between their images is known in advance, otherwise they need to be estimated. A good survey on image registration is (Zitova, 2003).

Once registered image couple is in hand, the PSF, which minimizes the difference between the low-resolution image and the high-resolution image filtered with the PSF, can be found by optimization techniques. If both imagers are on the same satellite, processing is simplified. For example, in (Bretschneider, 2002), the MTF of 18 m-resolution multispectral camera is found by comparing the sum of multispectral channels to 6 m-resolution panchromatic camera of MOMS-2P imager. It is also possible to use images from different sensors. For example, (Schowengerdt, 1985) used images from airborne platforms to determine Landsat-4 TM MTF, while (Latry, 2004) used similar images for SPOT-5 MTF. On the other hand, there are Wiener filter based techniques that estimate optimum MTF in the frequency domain (Bretschneider, 2001). One can refer to (Helder, 2004) and (Léger, 2004) for more information on on-orbit MTF determination methods.

### 3. MTF DETERMINATION OF BiLSAT CAMERAS

For determining the MTF of each BiLSAT multispectral channel, two different methods are used. The first one is based on finding the LSF first from which the MTF is derived. The second method compares BiLSAT images to images from other satellites with known PSF to find PSF of BiLSAT cameras. Then, the MTF can be calculated by Fourier transformation. In both methods, PSF is assumed to be linear and shift-invariant. BiLSAT cameras are frame type cameras as opposed to usual pushbroom imagers, so the PSF is assumed to be radially symmetric if we ignore motion blur due to movement of the satellite during integration. In Figure 1, expected contribution of motion, detector and optics to the MTF are given for green channel. The integration time for this channel is typically 0.78 msec, which gives 5.26 m of drift during integration time or  $1/5.36^{\text{th}}$  of a pixel, given 6.74 km ground track velocity. Corresponding MTF in Figure 1 justifies our assumption of radially symmetric PSF. The MTF of the lens used in the instrument is measured before integrated into the instrument and defines an upper limit for MTF of the optics.

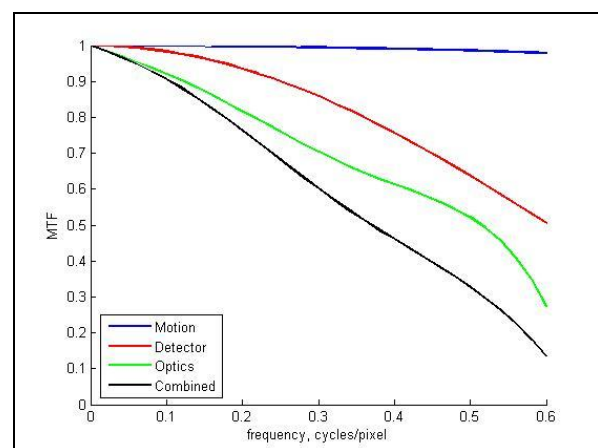


Figure 1. Various components of expected MTF for green channel

In the next two sub-sections both methods are explained in detail and the results are discussed. In following Sub-Section 3.3, the results are compared. The last sub-section describes the method used for MTF determination of BiLSAT panchromatic camera.

### 3.1 MTF from LSF

The first method for image-based MTF determination uses a sharp linear edge for estimating the Edge Spread Function (ESF), from which Point Spread Function (PSF) is obtained by differentiation.

#### 3.1.1 The Imaging Target

Since it is not practical to use specially made targets at low resolution, various natural and man-made almost linear structures with high-contrast are tried as imaging targets. Due to a temporary technical problem of the ground station, we had to use the archived images only. The best edge we could find for MTF determination is shown in Figure 2.

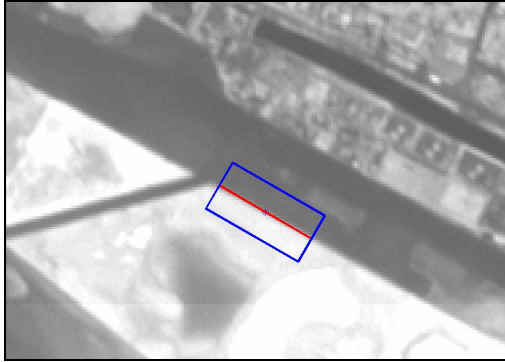


Figure 2. BiLSAT, Green, Abu Dhabi, 9 June 2005

#### 3.1.2 Accurate Edge Detection

For precise detection of the edges, a 2D edge model is fitted to manually picked linear edges. Sigmoid function

$$c(x, y) = a + b \frac{1}{1 + e^{-\lambda x}} \quad (1)$$

is used as edge model where

$$\begin{bmatrix} x' \\ y' \end{bmatrix} = \begin{bmatrix} \cos \alpha & \sin \alpha \\ -\sin \alpha & \cos \alpha \end{bmatrix} \begin{bmatrix} x \\ y \end{bmatrix} + \begin{bmatrix} x_0 \\ y_0 \end{bmatrix}, \quad (2)$$

$x_0$  and  $y_0$  is the center of the edge and  $\alpha$  is the edge orientation. The root-mean-square difference between the image and the model is minimized by simplex method and very accurate edge position, edge angle and high and low values at both sides of the edge are estimated (In total, 6 parameters are optimized including  $\lambda$ ). In Figure 2, accurate edge position is showed as overlaid on the original image. This process is repeated for each channel since the imagers are not perfectly aligned. In Figure 3, the detected edge is shown in 3D. It can be seen that the image is not perfectly uniform on especially the bright side.

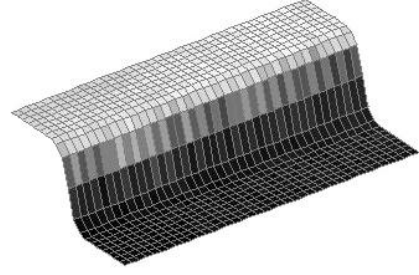


Figure 3. The edge in 3D, near-IR channel

#### 3.1.3 Projection and Curve Fitting

Once the edge is determined accurately, all the image samples around the edge are projected onto a line across the edge. Firstly the signal-to-noise ratio (SNR) is calculated as suggested in (Choi, 2003b), that is,

$$SNR = b / \sigma_n \quad (3)$$

where  $\sigma_n$  is the standard deviation of noise. The SNR for this PSF is found to be around or less than 50 depending on multi-spectral channel, while (Helder, 2003) states that PSF should be above 50 for accurate results. We have chosen parametric curve fitting, since it is more robust to noise. First, the error function,

$$erf(x) = \frac{2}{\sqrt{\pi}} \int_0^x e^{-x^2} dx, \quad (4)$$

is used as ESF model, which corresponds to a Gaussian PSF. Since this model is too simple, a polynomial fit is also performed. Lower order polynomials cannot follow the corner points while higher order polynomials have ripples due to noise as can be seen in Figure 4. For that reason we have used a new function that combine powerful sides of both functions:

$$c(x) = a + b erf\left(\frac{x - x_0}{\sigma\sqrt{2}}\right) + w(x - x_0) \sum_{i=1}^3 c_i (x - x_0)^{2i-1} \quad (5)$$

where  $w(x)$  is the Hanning window

$$w(x) = \begin{cases} \frac{1}{2} \left[ 1 + \cos\left(\frac{2\pi x}{s}\right) \right], & -s/2 < x < s/2 \\ 0, & elsewhere \end{cases} \quad (6)$$

and  $s$  is large enough to cover the transition zone. The error function follows general shape of the data and the residuals can be modeled by a lower order polynomial. The function can follow sharpest transitions and is robust to noise at the same time. The Hanning window guaranties that the PSF reaches zero at both ends. Only odd powers of the polynomial are used to force a symmetrical PSF. All parameters are determined by optimization.

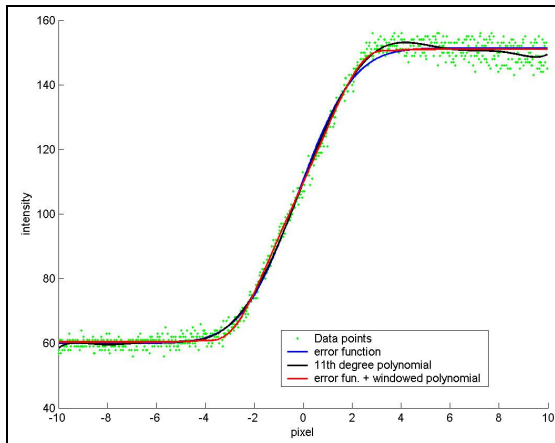


Figure 4. ESF curves for red channel

In Figure 5, error function, 11<sup>th</sup> order polynomial and the proposed function are shown at higher corner of the ESF.

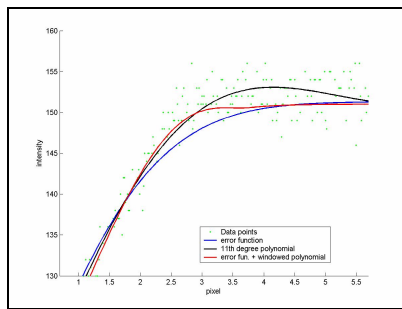


Figure 5. Different ESF models at higher corner

### 3.1.4 Calculating MTF and Results

The PSF curves calculated by differentiation from ESFs sampled at 1/16 pixel are shown in Figure 6. A 1024-point FFT is applied to the PSF. Resultant MTFs for all multispectral channels are shown in Figure 7.

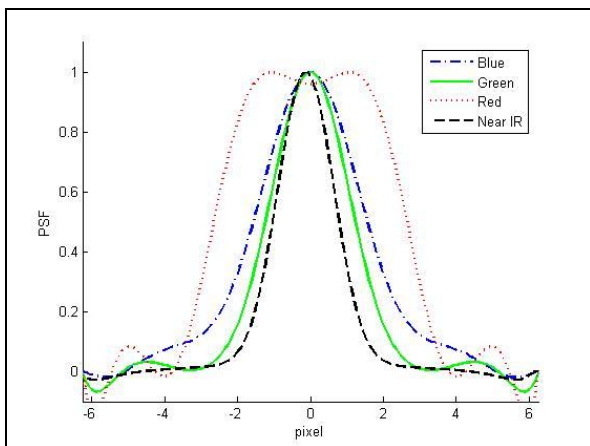


Figure 6. PSF curves for multispectral imager channels

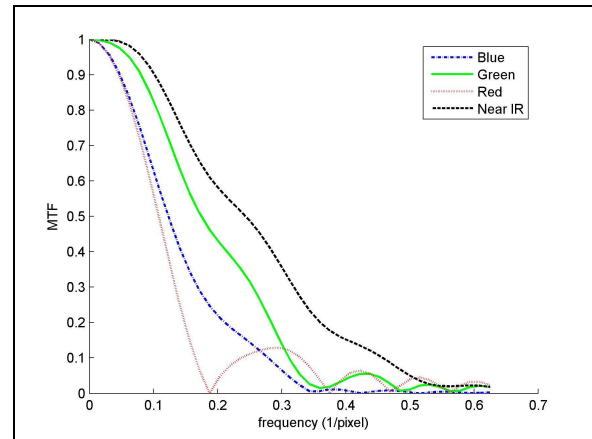


Figure 7. MTF curves for multispectral imager channels

## 3.2 MTF using High-Resolution Images

Second method is based on comparing BiLSAT images to 4 m-resolution multispectral IKONOS images whose PSF is already known. BiLSAT multispectral channels' filters are similar to corresponding filters of IKONOS. The method used is described in following sub-sub-sections.

### 3.2.1 Image Registration

Firstly, we need to register the images accurately to be able to compare them. Since they are not taken exactly from the same view angle, there can be parallax effects. We have chosen small and almost planar areas using digital elevation model of Adana city in Turkey to avoid effects of parallax. In Figure 8 and Figure 9, two such sub-images from BiLSAT and IKONOS are shown, respectively.

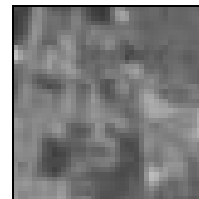


Figure 8. BiLSAT, Adana, Green, 11 February 2005, 40x40 cut



Figure 9. IKONOS, Adana, Green, 5 October 2004, Almost same area as Figure 8

Under the assumption of planarity and perfect perspective cameras, the transformation between the images is a planar projective homography with 8 degrees of freedom:

$$\begin{bmatrix} x_2 \\ y_2 \\ 1 \end{bmatrix} = \begin{bmatrix} h_{11} & h_{12} & h_{13} \\ h_{21} & h_{22} & h_{23} \\ h_{31} & h_{32} & 1 \end{bmatrix} \begin{bmatrix} x_1 \\ y_1 \\ 1 \end{bmatrix} \quad (7)$$

where  $(x_1, y_1)$  and  $(x_2, y_2)$  are the image coordinates of BiLSAT and IKONOS images, respectively. Besides the geometric transformation, radiometric correction is also necessary, since the radiometric responses of the sensors are not identical and the lighting conditions are different during image exposure. We have assumed a linear model that has 2 free parameters:

$$I_B = r_0 + r_1 I_I \quad (8)$$

where  $I_B$  and  $I_I$  are the image digital values of BiLSAT and IKONOS image, respectively and  $r_0$  and  $r_1$  are the correction parameters to be estimated.

### 3.2.2 Finding PSF by Optimization

After the planar homography and radiometric correction, a radially symmetric blur function,

$$g(x, y) = \frac{1}{2\pi\sigma_r^2} e^{-r^2/2\sigma_r^2} + w(r) \sum_{i=0}^4 c_i r^{2i} \quad (9)$$

where

$$r = \sqrt{x^2 + y^2} \quad (10)$$

and  $w(x)$  is the Hanning window as defined in Equation 6 is applied to the IKONOS image patch and the RMS difference between the transformed image and corresponding BiLSAT image patch is calculated. All 16 parameters (8 for homography, 2 for radiometry, 1 for the  $\sigma_r$  and 5 for  $c_i$ 's) are optimized together to minimize the RMS error using Powell algorithm. Initial values for geometric transformation are estimated using four tie-points, while initial values for radiometric correction are estimated based on histograms.

### 3.2.3 Results of Two Image Method

In Figure 10 and Figure 11, the PSF and MTF curves obtained by two-image method are shown, respectively. The PSFs need to be convolved with the PSF of IKONOS, however, it is ignored since its effect is very small. The blur function of Near-IR channel could not be estimated using the images of areas in Figure 8 and Figure 9, because there are contrast inversions, probably due to change in reflectance of vegetation from October 2004 to February 2005.

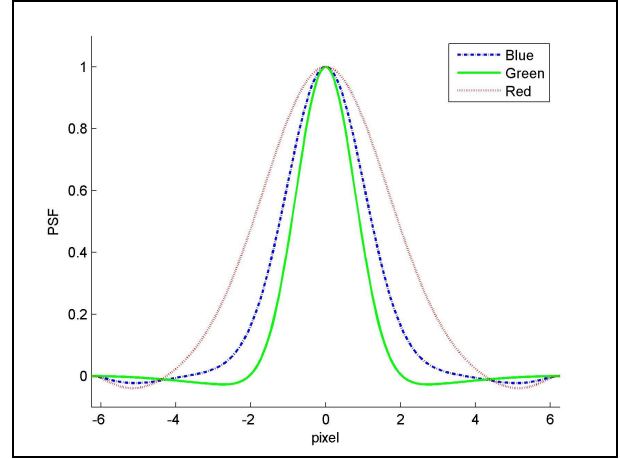


Figure 10. PSF by two-image method

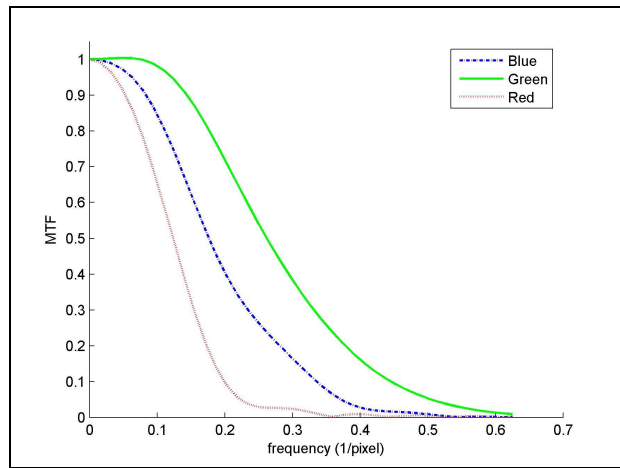


Figure 11. MTF by two-image method

### 3.3 Comparison of Both Methods

The MTF curves obtained by two methods are consistent, however, the estimated MTF curves from two-image method are better. The two-image method using images from different platforms involves many sources of error including, non-linear radiometric responses, differences of spectral sensitivities of compared imagers, physical changes of the scene during the time separation (especially vegetation), parallax effects, camera distortion which is not modeled by planar homography, errors in image registration, shadows (changes due to position of sun and due to different levels of occlusion) etc. It is also more demanding in terms of computation.

Although, the edge method is simpler, it is not easy to find large, very long, straight and high-contrast edges with uniform sides, at this resolution. We believe that the edge method is more reliable but this needs to be verified by other methods. Nevertheless, good results can be obtained from non-perfect targets.

### 3.4 MTF of Panchromatic Camera

In the BiLSAT image archives, appropriate panchromatic images for above-mentioned images were not available, so we have taken a different route to obtain a coarse estimate of the MTF. Although the GSD of panchromatic images is 2.22 times

higher than that of multispectral images, it is clearly seen by visual inspection that panchromatic images are highly blurred and more detail can be seen in multispectral channels. Hence, we have done the opposite of the usual practice and the panchromatic image is obtained by blurring the green channel image of the same scene, which has a larger GSD. A sharp target with minimum color content is chosen for that purpose. In Figure 12, both images are shown.

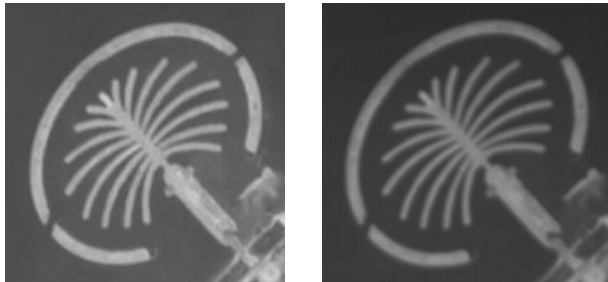


Figure 12. Target at Dubai. Left: green image, right: panchromatic image

The method described in Sub-section 3.2 is used to determine the best PSF that minimizes the RMS difference between panchromatic image and the green image filtered by that PSF. Resultant PSF is convolved with the PSF of green channel after proper resampling. Resultant MTF is shown in Figure 13.

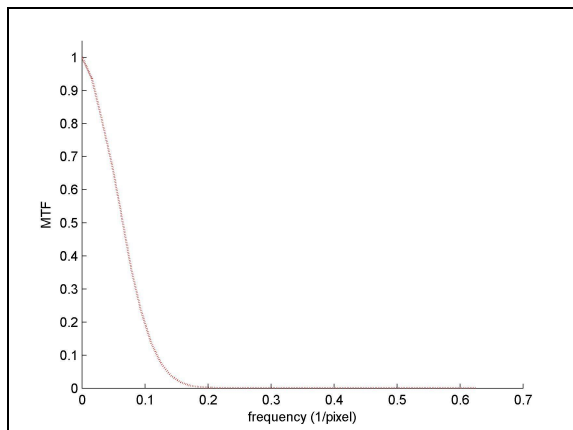


Figure 13. MTF of panchromatic channel

#### 4. CONCLUSIONS

In this study, two different methods are used to determine the MTF of four BiLSAT cameras that form the 28 m.-resolution multispectral imager. For the first method, which uses edge images for finding the ESF and hence the MTF, a new parametric blur model is proposed which is a good trade-off between non-flexibility and noise-sensitivity. A similar blur function is also used for two-image method, which uses a high-resolution image for MTF estimation. The results from both method are consistent, however, the MTF curves from second method are better, which can be due to various errors in the process.

Other than the near-infrared channel of BiLSAT multi-spectral imager, all cameras produce images blurred at various levels and over-all performance is below expected. This can be due to effects of vibration during launch, wrong calculation of offsets for vacuum environment or initial defocusing. The defocusing

of panchromatic imager is very severe, probably because the athermalization mechanism has failed in addition to other possible causes.

More experiments need to be done to verify the results and to determine the reasons of differences between the results of two method. Especially, edge method will be repeated with better targets and higher dynamic range of signals. Also, the temperature and focal plane position dependence need to be investigated.

#### REFERENCES

- Blonski, S., Pagnutti, M. A., Ryan, R. E., Zaroni, V., 2002. In-flight edge response measurements for high-spatial-resolution remote sensing systems, In: *Proc. SPIE Vol. 4814, Earth Observing Systems VII*, pp. 317-326.
- Braga, A. B., Schowengerdt, R. A., Rojas, F., Biggar, S. F., 2000. Calibration of the MODIS PFM SRCA for on-orbit cross-track MTF measurement. In: *Earth Observing Systems V, SPIE Proceedings Volume 4135*, San Diego, California, USA, pp. 71-79.
- Bretschneider, T., Bones, P.J., McNeill, S., Pairman, D., 2001. Image-based quality assessment on SPOT data. In: *Proceedings of the American Society for Photogrammetry & Remote Sensing, Sensor and Image Quality Considerations*.
- Choi, T., 2003a. Generic sensor modeling. In: *Proceedings of the 2003 High Spatial Resolution Commercial Imagery Workshop*, NASA/NIMA/USGS Joint Agency Commercial Imagery Evaluation Team, Reston, VA, USA, CD-ROM.
- Choi, T., 2003b. IKONOS Satellite on Orbit Modulation Transfer Function (MTF) Measurement using Edge and Pulse Method. *Master's Thesis*, South Dakota State University, USA.
- Delvit, J.-M., Leger, D., Roques, S., Valorge, C., 2004. Modulation transfer function estimation from nonspecific images. *Optical Engineering*. 43(6). pp. 1355-1365.
- Friedrich, J., Leloğlu, U. M., Tunalı, E., 2006. Radiometric camera calibration of BiLSAT small satellite: Preliminary results, In: *ISPRS Topographic Mapping from Space (with Special Emphasis on Small Satellites)*, Ankara, Turkey, CD-ROM.
- Helder, D., Choi, T., 2002. IKONOS Satellite on Orbit Modulation Transfer Function (MTF) Measurement using Edge and Pulse Method. *Technical Report*, South Dakota State University, USA.
- Helder, D., 2003. In-Flight Characterization of the Spatial Quality of Remote Sensing Imaging Systems Using Point Spread Function Estimation. In: *International Workshop on Radiometric and Geometric Calibration*, Gulfport, Mississippi USA.
- Helder, D., Choi, T., Rangaswamy, M., 2004. In-flight characterization of spatial quality using point spread functions. Post-Launch Calibration of Satellite Sensors. *ISPRS Book*

*Series – Volume 2*, eds. Morain, S. A., Budge, A. M., Balkema, A. A., London, pp. 151-170.

Forster, B. C., Best, P., 1994. Estimation of SPOT P-mode point spread function and derivation of a deconvolution filter. *ISPRS Journal of Photogrammetry and Remote Sensing*, 49(6), pp. 32-42.

Kohm, K., 2004. Modulation transfer function measurement method and results from the Orbview-3 high resolution imaging satellite. In: *Proceedings of ISPRS 2004*, Istanbul, Turkey.

Latry, C., Despringre, V., Valorge, C., 2004. Automatic MTF measurement through a least square method. In: *Proceedings of SPIE -- Volume 5570, Sensors, Systems, and Next-Generation Satellites VIII*, eds . Meynart, R., Neeck, S. P., Shimoda, H., pp. 233-244.

Léger, D., Duffaut, J., Robinet, F., 1994. MTF measurement using spotlight. *IGARSS '94*, Pasadena, California, USA.

Léger, D., Viallefont, F., Déliot, P., Valorge C. 2004. On-orbit MTF assessment of satellite cameras. *Post-Launch Calibration of Satellite Sensors. ISPRS Book Series – Volume 2*, eds. Morain, S. A., Budge, A. M. A. A. Balkema, London, pp. 67-76.

Luxen, M., Förstner, W., 2002. Characterizing image quality: blind estimation of the point spread function from a single image. *PCV 02. Proceedings of the ISPRS Comm. III - Symposium*, Graz, Austria.

Rauchmiller, R. F., Schowengerdt, R. A., 1988. Measurement of the Landsat Thematic Mapper MTF Using an Array of Point Sources. *Optical Engineering*, 27(4), pp. 334-343.

Tatian, B., 1965. Method for obtaining the transfer function from the edge response function. *Journal of the Optical Society of America*, 55(8), pp. 1014-1019.

Yüksel, G., Belce, Ö, Urhan, H, Gomes, L, Bradford, A, Bean, N., Curiel A., 2004. BILSAT-1: First year in orbit- Operations and lessons learned, *The 18th Annual AIAA/USU conference on small satellites*, Logan, Utah, USA.

Zitova, B., Flusser, J., 2003. Image registration methods: a survey. *Image and Vision Computing*, 21, pp. 977-1000.

## ACKNOWLEDGEMENTS

The BiLSAT microsatellite flight model has been designed and constructed by Surrey Satellite Technology Limited for TUBITAK-SPACE of Turkey in conjunction with engineers from TUBITAK-SPACE during a collaborative program comprising the manufacture of the BiLSAT microsatellite and training at the Surrey Space Centre, University of Surrey, Guildford, Surrey GU2 5XH, England.